





Cite this: *Mater. Horiz.*, 2022, 9, 1935

Received 5th March 2022,
Accepted 21st April 2022

DOI: 10.1039/d2mh00281g

rsc.li/materials-horizons

An ultrastretchable, high-performance, and crosstalk-free proximity and pressure bimodal sensor based on ionic hydrogel fibers for human-machine interfaces†

Haojun Ding,^a Zixuan Wu,^a Hao Wang,^a Zijing Zhou,^a Yaoming Wei,^a Kai Tao,^b Xi Xie ^a and Jin Wu ^{*a}

The traditional human-machine interaction mode of communicating solely with pressure sensors needs modification, especially at a time when COVID-19 is circulating globally. Here, a transparent, stretchable, resilient, and high-performance hydrogel fiber-based bimodal sensor is fabricated by using a polyacrylamide-alginate double network hydrogel, which features high sensitivity (3.17 cm^{-1}), wide working range (18 cm), fast response/recovery speeds (90/90 ms) and good stability in proximity sensing, and impressive pressure sensing performance, including high sensitivity (0.91 kPa^{-1}), short response/recovery time (40/40 ms), low detection limit (63 Pa) and good linearity. Moreover, the response switch between proximity/pressure modes is measured and non-interfering dual-mode detection is achieved. Notably, the stretchable bimodal sensor is capable of working under 100% tensile strain without degrading the sensing performance. Specifically, the proximity sensor shows good immunity to the strain, while the pressure sensitivity is even promoted. Furthermore, the sensor is tough enough to work normally after punctures from a knife and strikes from a wrench. Notably, the sensor can be used for gesture recognition and subtle pressure detection, such as small water droplets (10 mg), wrist pulse, etc. A 3×3 array is further shown for accurate spatial sensing and location identification, verifying the feasibility of its practical application.

1. Introduction

With the continuous development of digitization and industrialization of society, human-machine interfaces (HMIs), soft robots, and wearable electronics have attracted more and more

New concepts

Conventional proximity/pressure bimodal sensors lack the stretchability and toughness to work under a harsh environment and struggle to achieve synchronous detection and differentiation of proximity and pressure. Herein, we prepare highly stretchable ionic hydrogel fibers through a facile template method, to fabricate a crosstalk-free proximity/pressure bimodal sensor by crossing two fibers and encapsulating them with a stretchable elastomer, endowing the sensor with excellent resilience and ultrastretchability. Compared with previous proximity/pressure bimodal sensors, our sensor displays superior performance, including higher sensitivity, fast response/recovery speeds, wide working range, etc. The sensor can work normally under harsh environments, such as large tensile strain (100%) and knife punctures and wrench strikes. Also, we successfully realize crosstalk-free detection and differentiation of proximity and pressure due to the higher sensitivity of pressure than that of proximity. Furthermore, the response switch between proximity/pressure modes can be detected by monitoring the turning point of the capacitance curve, which ensures the accurate recognition of two stimuli and the operation of the bimodal sensor with minimal interference. In brief, this research offers a novel device structure and superior performance, which opens up various opportunities related to human-machine interaction (e.g., gesture recognition), and non-invasive healthcare (e.g., dysphagia and cardiovascular disease monitoring).

attention.^{1–5} In particular, at a time when COVID-19 is ravaging the world, how to prevent it through safe HMIs has become a problem that needs to be solved. However, traditional HMIs are mainly accomplished through direct human touches with the help of single-functional pressure sensors.^{6–10} While the pressure pattern is very accurate at communicating the user's intentions, it is unable to respond to approaching objects, which greatly limits the scope of applications. For instance, robots fail to detect objects in the dark and take early action.¹¹ Moreover, it causes viruses to spread from person to person easily.^{12,13} Therefore, more contactless interactions are needed. Recently, proximity sensors have been gradually used in wearable devices and robots because of their ability to detect responses without physical contact.^{14,15} Though the mechanisms of contactless sensors

^a State Key Laboratory of Optoelectronic Materials and Technologies and the Guangdong Province Key Laboratory of Display Material and Technology, School of Electronics and Information Technology, Sun Yat-sen University, Guangzhou 510275, China. E-mail: wujin8@mail.sysu.edu.cn

^b Ministry of Education Key Laboratory of Micro and Nano Systems for Aerospace, Northwestern Polytechnical University, Xi'an 710072, China

† Electronic supplementary information (ESI) available. See DOI: <https://doi.org/10.1039/d2mh00281g>

mainly include magnetic induction, infrared light, *etc.*, the proximity sensor based on capacitance measurement provides a more convenient and inexpensive way.^{16–18} As application scenarios expand, more and more devices are required to detect both contact physical stimuli and contactless approaches at the same time. Therefore, finding a simple and effective method to combine capacitive pressure and proximity sensing capabilities in one single device can greatly enrich the function of the devices.

When integrating pressure and proximity sensors into epidermal electronics, flexibility and stretchability are key factors to improve the lifetime of products and ensure their comfort of wearing. For example, when human joints move, the corresponding skin will stretch, and stretchable epidermal electronics attached to human skin can move together with the skin to avoid discomfort. However, traditional materials, such as indium tin oxide (ITO), are vulnerable to strains due to their brittleness. Moreover, these materials are complicated in the preparation process and costly.¹⁹ Pei *et al.* reported a bimodal capacitive fiber sensor prepared from silver nanowires (AgNWs) and bacterial cellulose (BC) with high sensitivity and a large detection range.²⁰ Nevertheless, the AgNW-BC fiber only owned a limited elongation strain of 3.0%, which is not enough for the application of the robot and human joints with large strains. Tang *et al.* developed a capacitive sensor for proximity/pressure sensing based on PEDOT:PSS/SWCNT hybrid electrodes.²¹ Since all components of the sensor, including the encapsulation layer, dielectric, and electrode, were stretchable, no significant change was observed in the process of a finger approaching at a distance of ~ 2 cm and pressure loading of 2 and 2.4 kPa under the strains from 0 to 40%. Nevertheless, 40% strain is relatively small compared with the 100% deformation of a soft robot or human joint strain, which requires further improvement. Also, the work failed to systematically explore the effect of strain on pressure and proximity, which is very important because sensors integrated into flexible robots often need to work under stretching states. In addition to stretchability, transparency is also a significant property to achieve the next-generation electronic devices, including electroluminescent skin, new energy devices, *etc.*^{22–24}

For multifunctional sensors, a key aspect is to achieve synchronous detection and differentiation of proximity and pressure. Many previous articles have only mentioned that their devices can detect both proximity and pressure without mentioning how to avoid the response induced by proximity in pressure sensing mode.^{25,26} For example, Wang *et al.* reported a dual functional transparent film with a substrate of PET.¹¹ Due to the toughness of the PET substrate, when the finger presses on the sensor, the distance between the finger and the sensor remains the same. Thus, the capacitance induced by a change in proximity can be negligible. However, it would be different for soft substrates (*e.g.* Ecoflex or PDMS) because when they are pressed, the capacitance induced by proximity would change due to the compression and deformation of elastomers, leading to inaccurate pressure sensing. Unfortunately, few reports have mentioned this situation. Considering that the piezoresistive

sensor is not responsive to proximity, Park *et al.* distinguished proximity and pressure using resistance for pressure detection and capacitance for proximity detection.²⁷ Unfortunately, two sensors including a capacitive sensor and a piezoresistive sensor are needed for the distinction. Also, the sensors are opaque, limiting their application for electronic skin. Therefore, it is still challenging to prepare a bimodal sensor that can normally work under large strain and achieve simultaneous detection of proximity and pressure with non-interference, high transparency and resilience.

Recently, conductive hydrogels have been widely employed to construct stretchable and wearable electronics including various sensors (*e.g.* gas, temperature, strain, pressure, *etc.*) attributed to the impressive advantages of good stretchability, high transparency, self-healing ability, and biocompatibility.^{28–34} Traditional hydrogels have been troubled with evaporation-induced structural dehydration and freezing-induced hardening issues at sub-zero temperatures.³⁵ Fortunately, the introduction of anti-freezing agents (such as salt or alcohol) has greatly solved these problems, making the hydrogel a promising candidate material for fabricating ionotronics with a long life.³⁶

Fiber-shape sensors are promising in wearable devices due to their advantages, such as lightweight, ultra-flexibility, and weavability, which have been widely integrated with textiles to fabricate smart textiles for human health monitoring.³⁷ So far, hydrogel fiber-based stretchable proximity/pressure sensors have seldom been reported. Herein, we demonstrated a facile method of fabricating an ionic hydrogel fiber-based sensor that is capable of crosstalk-free detection of proximity and pressure. The hydrogel fibers were synthesized from acrylamide (AAM) and sodium alginate with a template method, which were then encapsulated in a layer of Ecoflex. The two aforementioned fibers were perpendicularly crossed to form a capacitor, where the hydrogel fibers and the Ecoflex acted as electrodes and the dielectric layer, respectively. Owing to the high elasticity of the dielectric layer, the bimodal sensor displayed impressive pressure sensing performance, including high sensitivity (0.91 kPa^{-1}), fast response/recovery time (40/40 ms), and low detection limit (63 Pa), which enabled the sensor to be applied in subtle physiological signal detection, such as the detection of a wrist pulse, swallowing, and vocalization. Also, the bimodal sensor showed good proximity sensing ability with a wide detection range (18 cm), short response/recovery time (90/90 ms), and high sensitivity ($3.17\% \text{ cm}^{-1}$), enabling it to accurately detect the proximity of a human hand, including the number of fingers and different gestures. Furthermore, the bimodal sensor could normally work even under the strain of 100%. The large strain exhibited little effect on the proximity sensing, but greatly improved the pressure sensing ability, allowing for reliable proximity and pressure monitoring at highly deformed states. What is more, our sensor can achieve simultaneous detection of proximity and pressure, leading to accurate pressure detection with the avoidance of proximity interference. Notably, the bimodal sensor showed good resilience to the damage by outer forces. After the punctures of a knife and the impacts of a wrench, the bimodal sensor also responded

normally to the approaching hand and finger pressure. With these intriguing performances, the bimodal sensor has been applied for various practical applications, such as gesture recognition and the real-time monitoring of various physiological activities (*e.g.*, swallowing, speaking, wrist pulses, *etc.*) as a wearable device.

2. Results and discussion

2.1 Characterization of the hydrogel fiber and device

Fig. 1a shows a schematic diagram of our capacitive fiber-based bimodal sensor, which can work at proximity and pressure modes. The sensor is fabricated with two crossed hydrogel fibers encapsulated by an Ecoflex layer. The intersection of two hydrogel fibers is regarded as a capacitor, where the Ecoflex and the hydrogel serve as the dielectric layer and electrodes, respectively. Capacitance changes when a conductor (*e.g.*, a human hand) is approaching a sensor or when the sensor is compressed. A highly stretchable hydrogel fiber with a diameter of 660 μm was synthesized *via* the mold of a glass capillary (Fig. 1b). The details are described in the experimental part. Specifically, the hydrogel precursor solution was injected into a glass capillary with a syringe, which was then sealed to avoid the formation of bubbles during the heating process. During the injection process, the formation of bubbles should be minimized, otherwise, the hydrogel fibers will be easy to break when stretched. The glass capillary was then put into an oven and heated at 65 $^{\circ}\text{C}$ for two hours to realize the polymerization of AAm. Here, *N,N*-methylenebisacrylamide (MBA) and ammonium persulfate (AP) functioned as a cross-linker and thermal initiator, respectively, for the covalent crosslinking of polyacrylamide (PAM). After that, the fiber was taken out from the glass capillary and soaked in 1 M CaCl_2 for 30 min to get ionically crosslinked alginate. So far, a double-network (DN) hydrogel fiber with toughness and high stretchability was achieved.

Because hydrogel fibers can easily lose water, they were soaked in 50 wt% LiBr for 15 min to improve the anti-drying ability by virtue of the strong ionic hydration effect of LiBr.³² As can be seen in Fig. S1 (ESI[†]), the pristine hydrogel fibers lost 90% of their weight after 48 hours, while the hydrogel fibers soaked in 50 wt% LiBr solution did not become lighter, and even became heavier due to the adsorption of moisture from the ambient air, showing good resistance to dryness. The ultrastretchable and anti-drying hydrogel fibers were then utilized for the fabrication of a bimodal sensor (Fig. 1c). Firstly, hydrogel fibers were tied with silver wires at both ends and dipped into the Ecoflex prepolymer for 10 s to form the encapsulation layer of Ecoflex, which acted as the dielectric layer of the capacitor. Then, the two aforementioned fibers were placed perpendicular to each other on an Ecoflex film and finally fixed to the film with Ecoflex prepolymer to avoid the slippage of the two fibers when the film was stretched. Finally, the hydrogel fiber-based bimodal sensor was obtained, which can normally work under stretching states. The cross-sectional

profile of the sensor is illustrated in Fig. S2 (ESI[†]). The excellent stretchability of the device is because of the excellent stretchability of both the hydrogel fiber and the Ecoflex film. In Fig. 1d and e, the hydrogel fiber could be stretched to as large as 1400% strain due to the effective energy dissipation caused by the DN structure.³⁸ The elastic modulus of the hydrogel fiber was calculated to be 70 kPa within the linear range from 0 to 150% strain, reflecting the high toughness. Thanks to the transparency of the hydrogel and the thin Ecoflex, the device also exhibited high transparency, which was evidenced by placing the device on a printed badge of SYSU as background (Fig. 1f). Notably, the badge could be seen with the coverage of our sensor. Another kind of sensor fabrication method of using two Ecoflex films to sandwich the fibers and cover the fibers, respectively, was also explored, which was not as good as the method mentioned above because the sensor made in this way failed to differentiate proximity and pressure, indicating the important role of the thin Ecoflex layer and the device structure in the sensing performance (Fig. S3, ESI[†]).

2.2 Proximity sensing

To measure the proximity sensing performance of the bimodal sensor, a human finger approached the sensor placed in a fixed position. The vertical distances between the finger and the sensor were calibrated using a ruler. It was interesting to note that when a finger approached the sensor, the capacitance declined rapidly. The mechanism can be explained in Fig. 2a. There are two kinds of capacitance that need to be noticed: the mutual capacitance C_m between two perpendicularly crossed fibers, which is the parameter we measured in the whole process, and the capacitance C_f between the finger and the upper fiber of the sensor, which is grounded through the human body. Since the human body serves as a grounded conductor, electric field lines of the capacitor can pass through the body into the ground, which reduces the strength of the electric field associated with the capacitor plate, thus reducing the charge stored in the capacitor. This is equivalent to the process that capacitor C_m is charging C_f , resulting in a decrease in C_m . And the smaller the distance between the human hand and the sensor is, the more charges flow from C_m to C_f , so the reduction of C_m become greater.^{19,39}

Results shown in Fig. 2b illustrate the high sensitivity of the fiber proximity sensor, which is defined as $(\Delta C/C_0)/\Delta d$ and calculated as 3.17% cm^{-1} , where Δd is the change of the vertical distance between the sensor surface and the finger. We also tested the capacitance variation as the vertical distance changed during a finger leaving and approaching process (Fig. 2c). It could be seen that the two curves highly overlapped at a distance of 0–8 cm, showing good reversibility and minimal hysteresis of the sensor. For the accuracy and convenience of the cyclic experiment, we fixed a conductor on one end of the motion controller (SC 300), which could also induce the capacitance change of the sensor, while the bimodal sensor was on the other end. The vertical distance between the sensor and the conductor was controlled by a computer, which was changed from 0 to 1 cm for 200 cycles. The response was

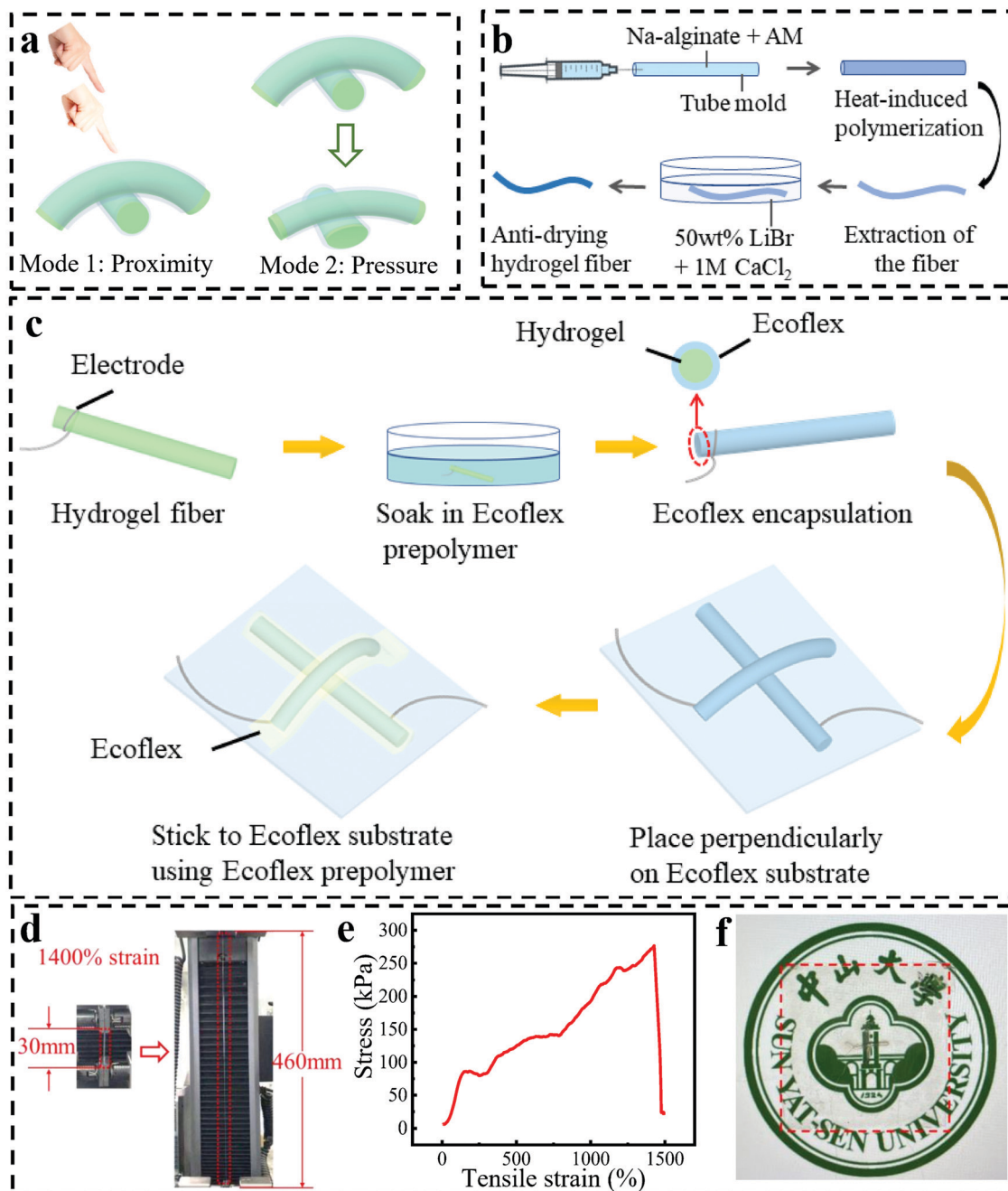


Fig. 1 (a) Schematic diagram of the capacitive fiber-based bimodal sensor, which can work at both proximity and pressure modes. (b) The preparation method of the anti-drying and tough hydrogel fiber. (c) The fabrication process of the bimodal sensor. (d) Photographs of the hydrogel fiber at 0% and 1400% tensile strains, respectively. (e) Stress-strain curve of the hydrogel fiber. (f) Photograph of the transparent sensor placed on a printed badge of SYSU as a background.

reproducible and stable and could be seen from a magnified image, demonstrating impressive cycling stability (Fig. 2d and e). We also conducted a test with a step of 1 cm at different distances from the sensor. It could be seen that the farther away from the sensor surface, the smaller the capacitance changed (Fig. S4, ESI†). This is because the electric field lines of the capacitor C_m are sparse at places far away from the sensor, so fewer electric field lines pass through the conductor into the ground, leading to the smaller capacitance change.

The high sensitivity and good stability of the sensor in proximity sensing make it suitable for hand gesture recognition. Different numbers of fingers were suspended at about 5 cm height above the sensor. As can be seen in Fig. 2f and Movie S1 (ESI†), the absolute value of the capacitance variation increased linearly as the number of fingers increased, which was attributed to the increasing effective overlapping area between the sensor and fingers. Based on this, we could further identify many kinds of meaningful gestures including “No. 1”, “YEAH”, “OK” and so

on, confirming the great potential of the sensor in gesture recognition applications (Fig. 2g and Movie S2, ESI†). The response of the sensor to the vertical movement of the palm at different speeds was also tested (Fig. 2h and Movie S3, ESI†). At the slow and medium speeds, the proximity sensor showed a stable response. At the fast speed, the response differed in three cycles, which was caused by the different distances between the palm and the sensor surface due to the fast-moving palm. It was clear that the proximity sensor displayed a rapid response to the fast-moving objects from the sharp peak in the curves. The response and recovery time of proximity sensing in the fast-moving cycle were measured to be 90 and 90 ms, which was limited by the speed of the human hand and could be shorter for the faster-moving object (Fig. 2i). To display the proximity sensing of the bimodal sensor, a video showing the capacitance change of the sensor to the approach of a human hand at

different speeds on the side of the sensor is also provided (Movie S4, ESI†).

2.3 Pressure sensing

In addition to high sensitivity, fast response/recovery speeds, and good stability in proximity detection, the bimodal sensor can also accurately measure the pressure based on the deformation of the hydrogel fibers and elastomer. A schematic diagram of the capacitor consisting of two perpendicularly crossed fibers was drawn to explain the working mechanism of the pressure sensing. Here, we introduce a parallel-plate configuration for illustration: $C = \epsilon S / 4\pi kd$, where C is the capacitance composed of two fibers and Ecoflex, ϵ is the dielectric constant of the elastomer Ecoflex layers, k is the electrostatic constant, S is the effective overlap area of two hydrogel fibers, and d is the thickness of the Ecoflex between

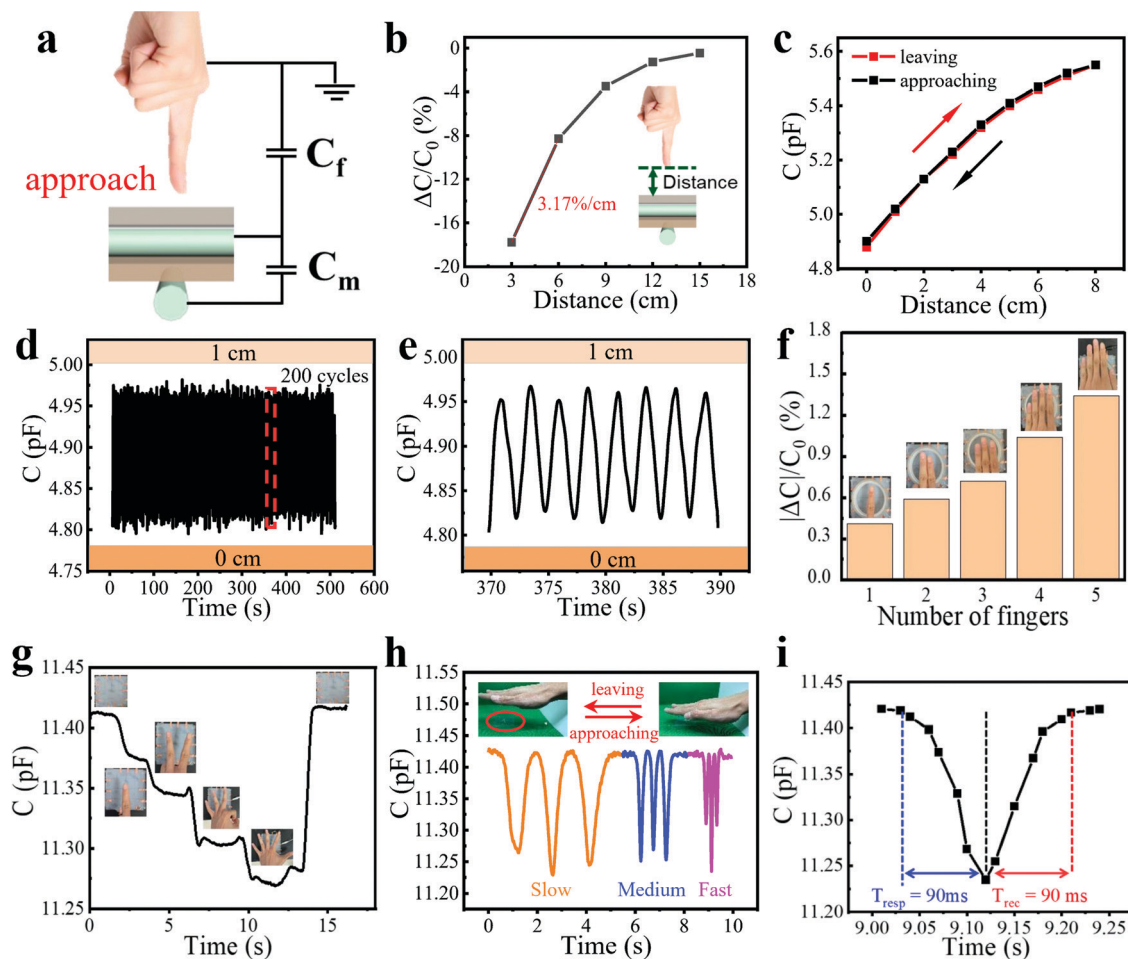


Fig. 2 Proximity sensing performance and the gesture recognition of the bimodal capacitive sensor. (a) Schematic of the proximity sensing mechanism. (b) Relative capacitance change responding to an approaching finger at different distances. Inset: Schematic diagram showing the approaching finger towards the sensor. (c) Capacitance versus distance during a finger leaving–approaching cycle. (d) Capacitance change of the sensor to repeated proximity sensing for 200 cycles, showing good stability of this proximity sensor. (e) Magnified image of Fig. 2d from 370 to 390 s. (f) Relationship between $|\Delta C|/C_0$ and the number of fingers at about 5 cm height above the sensor. Inset: Pictures of a different number of fingers above the sensor. (g) Capacitance change of the sensor to different gestures. Inset: Pictures of meaningful gestures including “No. 1”, “YEAH”, “OK”, etc., above the sensor. (h) Capacitance changes to the vertical movement of the palm at different speeds. Inset: Photos of the palm approaching and leaving the sensor. (i) Response/recovery time of proximity sensing in the fast-moving cycle of Fig. 2h.

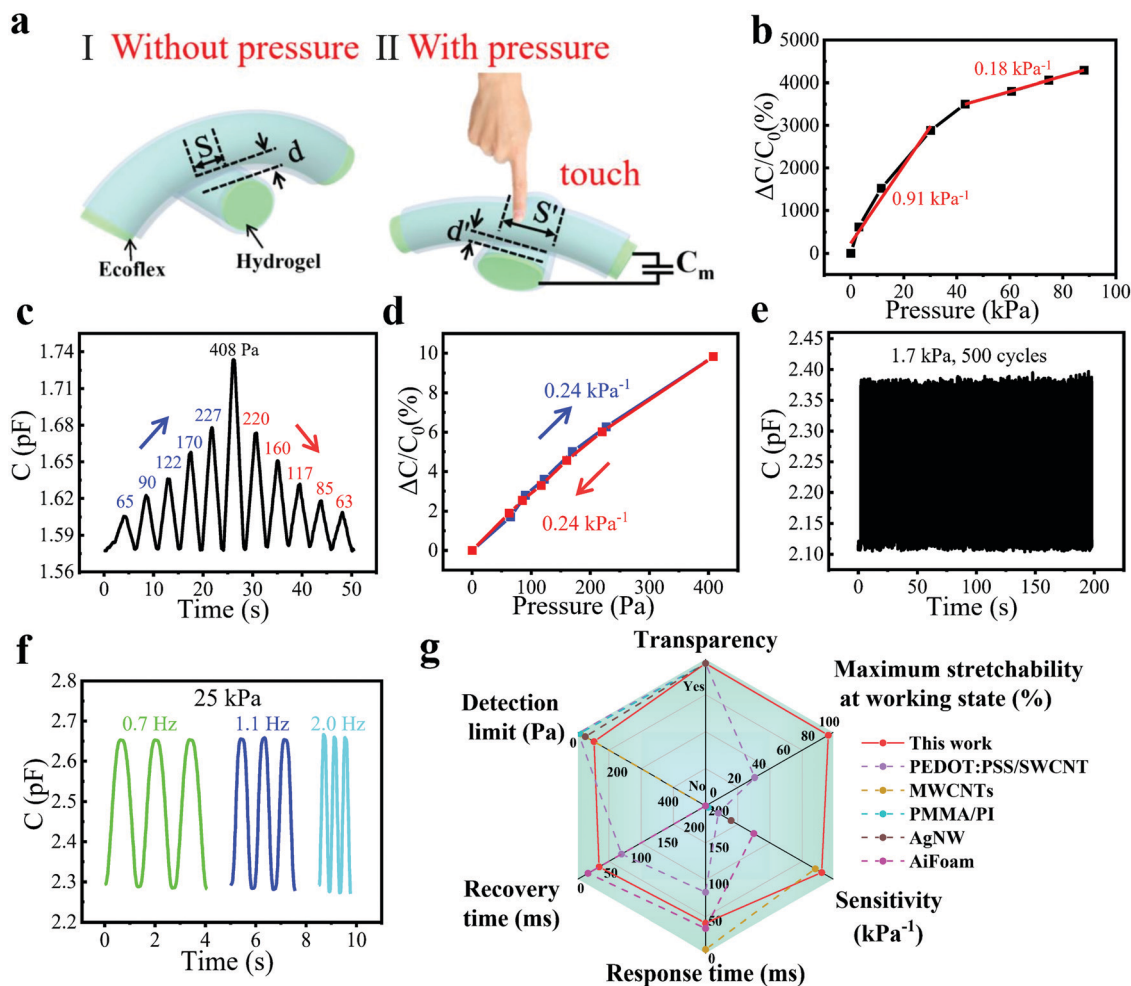


Fig. 3 The pressure sensing performance of the bimodal capacitive sensor. (a) Schematic diagram of the pressure sensing mechanism of a bimodal sensor. I and II are sensor states before and after applied pressure, respectively. (b) Relative capacitance change responding to different pressures. (c) Real-time capacitance change to varying subtle pressures. (d) Pressure sensitivity in the pressure range of 0–408 Pa was analyzed from the response vs. pressure curve. (e) Capacitance change under a pressure of 1.7 kPa for 500 cycles. (f) Capacitive response of the sensor to the pressure of 25 kPa at different frequencies (0.7 Hz, 1.1 Hz, and 2 Hz). (g) Capability radar diagram of state-of-the-art pressure sensors.

the fibers. When the pressure applied to the sensor increases gradually, the thickness of the Ecoflex between two fibers decreases to d' , while the overlap area increases to S' , leading to higher capacitance (Fig. 3a).

The pressure sensitivity is defined as $(\Delta C/C_0)/\Delta P$, where ΔC and C_0 are the change of capacitance and the initial capacitance of the sensor, respectively, while ΔP is the pressure change. The pressure sensitivity was calculated to be as high as 0.91 kPa^{-1} in the pressure range from 0 to 30 kPa and 0.18 kPa^{-1} in the pressure range from 43 to 88 kPa (Fig. 3b). Meanwhile, the sensor is also sensitive enough to detect subtle pressure. To demonstrate it, the sensor was applied with a series of subtle pressures from 65 Pa to 408 Pa and then back to 63 Pa, as shown in Fig. 3c. It is very easy for the sensor to detect pressure as low as 63 Pa, which we believe is not the limit of detection because of the high capacitance response (1.4%) at 63 Pa. Meanwhile, the capacitance varied linearly with the increase/decrease of pressure during the above process and the sensitivity was calculated as 0.24 kPa^{-1} , showing good linearity and

reversibility, as well as small hysteresis (Fig. 3d). A cycling experiment was also conducted to evaluate the stability of pressure sensing. During 500 repeated cycles under a pressure of 1.7 kPa (Fig. 3e), the pressure responses of each cycle were close to each other, which can be seen more clearly in the magnified image (Fig. S5, ESI†). Pressure sensors generally work at different pressure frequencies, so it is necessary to measure the frequency response. Fig. 3f displays the frequency response at a pressure of 25 kPa. The response stayed similar at frequencies ranging from 0.7 to 2 Hz, demonstrating the frequency-independent pressure sensing, which was attributed to the fast response/recovery speeds. This allows the application of sensors in a wide range of scenarios. We also tested the response of the sensor to humidity. As shown in Fig. S6 (ESI†), the capacitance of the sensor barely changed when a volunteer exhaled towards the sensor. This was because the hydrogel fibers were wrapped around by the Ecoflex elastomer, which blocked moisture from entering and thus endowed the sensor with good humidity immunity. In general, the bimodal sensor

features excellent pressure sensing performance, including high sensitivity (0.91 kPa^{-1}), short response/recovery time (40/40 ms), low detection limit (63 Pa), and good linearity, and thus compares advantageously with existing capacitive bimodal sensors (Fig. 3g and Table S1, ESI†).

To further demonstrate the potential of our sensors in measuring tiny pressures, we applied them in different scenarios. For instance, the sensor was placed on a tough table and pressed lightly with a finger. Three distinct peaks appeared on the capacitance curve, indicating that the sensor is ultrasensitive to

low pressures such as finger pressing (Fig. 4a). The increased pressure produced an augmented response. The response and recovery times were measured to be 40 and 40 ms (Fig. 4b), respectively, which were much shorter than those of human skin (100 ms).⁴⁰ To further demonstrate this, we replaced the tough table with a movable screen of a laptop (Movie S5, ESI†). The transparent sensor was attached to the screen and pressed by a finger with varying amounts of force. A small shake on the screen reflected subtle pressure from the finger. As can be seen, the sensor is highly sensitive to small pressures because of its high

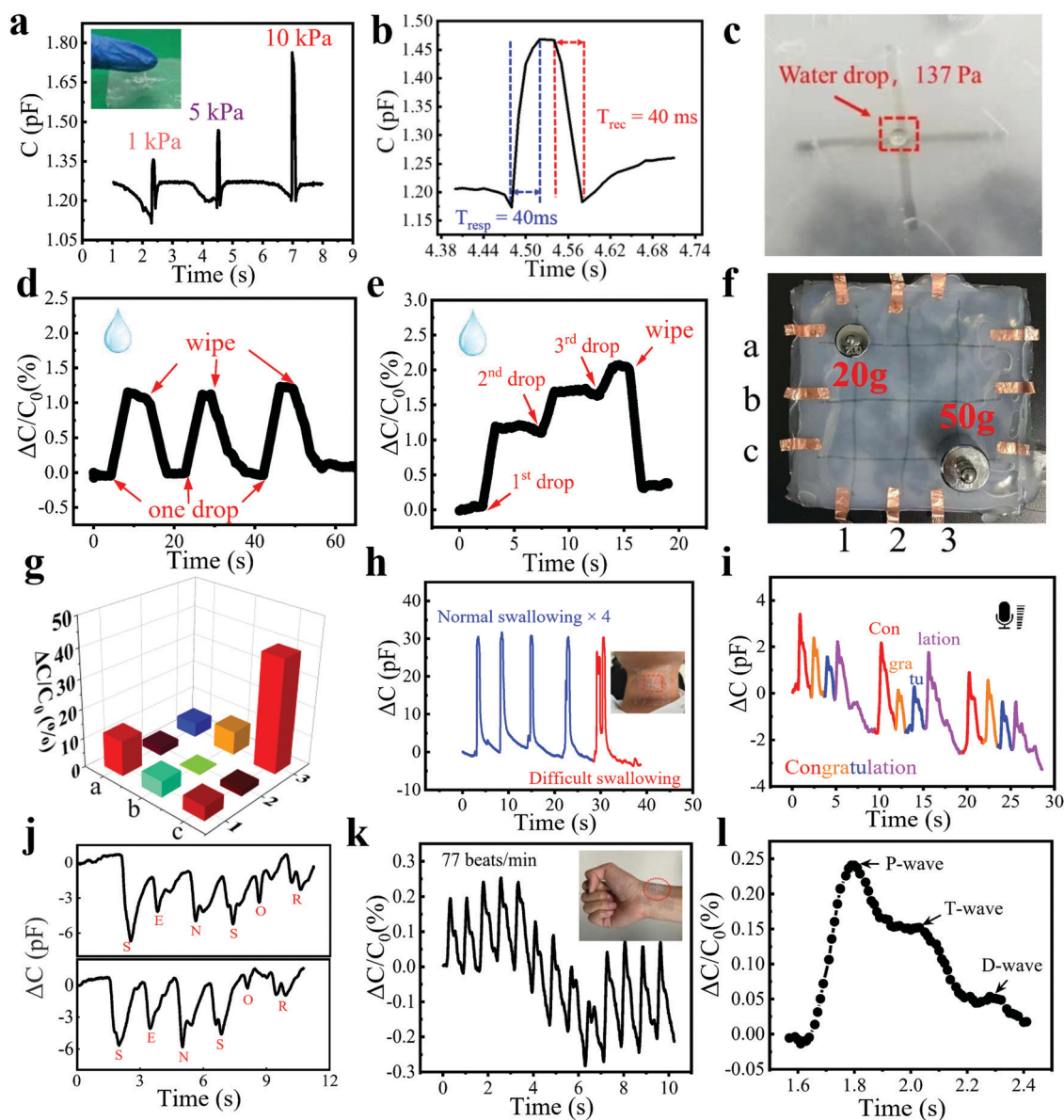


Fig. 4 Practical applications of the pressure sensor. (a) Capacitance variation when pressing with different pressures using a finger. Inset: Photo of a finger touching the sensor. (b) Fast response and recovery time of the sensor. (c) A picture showing the detection of a water droplet on the sensor. (d) Similar response to repeated dropping and wiping of one water drop on the surface of the sensor. (e) Real-time response to three successive drops of water on the sensor and their removal at the end. (f) Picture of placing a 20 g and a 50 g weight on the 3×3 sensor array. (g) Pressure mapping result upon placing a 20 g and a 50 g weight on the sensor array. (h) Dynamic response to repeated normal swallowing for four cycles and subsequent one difficult swallowing cycle. Inset: Photograph showing the stretchable sensor attached to the throat of a volunteer. (i) Capacitance change when speaking "congratulation". (j) Capacitance change when spelling "sensor" twice. (k) Detection of a wrist pulse. Inset: Photograph showing the wearable sensor attached to the wrist. (l) Waveform of a single pulse extracted from Fig. 4k.

sensitivity. The ultrafast response time is attributed to the high elasticity of Ecoflex because it allows the sensor to recover to its original state rapidly after the withdrawal of pressure.

Furthermore, the fiber sensor owns excellent performance in sensing subtle pressure changes brought about by lightweight objects such as a little water droplet or a small leaf. Fig. 4c shows a water droplet weighing 10 mg placed on the sensor surface, which was dropped from a height of 20 cm above the sensor. We conducted two experiments to demonstrate the real-time response of the sensor to water droplets. As shown in Fig. 4d, a water droplet was dropped onto the sensor and then wiped off, which was repeated for three cycles. Each water droplet led to a similar capacitance change of $\sim 1\%$. Then, three water droplets were continuously dropped onto the sensor surface drop by drop and wiped off using a piece of paper at the end (Fig. 4e). The response increased linearly with the increase of droplet number and then recovered well after the droplets were wiped off. Because the water droplets on the surface of the sensor were not completely removed, the curve did not return to its original position. To demonstrate the potential for HMI and e-skin, a large-area and flexible sensor matrix was fabricated to show the pressure mapping ability of the bimodal sensor. Fig. 4f shows the proof-of-concept 3×3 sensor array with an area of $10 \times 10 \text{ cm}^2$. Two different weights (20 and 50 g) were placed at the intersection of the fibers (a_1 and c_3) of the sensor array. The response brought by the heavier weight was much larger than the other, while other sites of the array without weight displayed almost no response, showing that the array can accurately measure the applied pressure location (Fig. 4g). In our future work, the resolution of the sensor array can be further improved by increasing the intersection number of fibers and minimizing the size of the pixel elements, which endows it with great potential in the applications of wearable devices and HMI.

Wearable and flexible sensors are an urgent need for HMI and physiological signal detection, such as the detection of swallowing, vocalization, and a wrist pulse, which are enabled by this ultrasensitive fiber-based wearable pressure sensor. The high stretchability and sensitivity enable the accurate detection of these physiological activities by conformally attaching to human skin. Nowadays, more and more people are suffering from a stroke, and difficulty swallowing or dysphagia is a common feature of it, which is hard to timely spot, especially for elderly people living alone.^{41,42} To illustrate the potential of our sensor in detecting dysphagia, the as-prepared wearable sensor was attached to the throat of a volunteer. Because the sensor was placed on top of the prominentia laryngea of the volunteer, there was only one peak when the volunteer swallowed normally for one time, which can be seen on the blue line in Fig. 4h. However, when a volunteer who had dysphagia swallowed once, several peaks appeared on the red curve due to the repeated back-and-forth movements of the prominentia laryngea, which facilitates the timely diagnosis of a stroke. Furthermore, the sensor can be used to differentiate the pronunciation of English words, such as the reading of "congratulation" and the spelling of "sensor" (Fig. 4i and j).

When a similar pronunciation appeared repeatedly, the sensor showed the same and stable pattern, indicating the potential application of the sensor for voice recognition. Fig. 4k demonstrated the real-time radial pulse waveform of a 26-year-old volunteer. The radial pulse was measured to be 77 beats per min, which is consistent with the normal radial pulse value of a healthy adult at rest.⁴³ Because our sensor can detect both pressure and proximity of conductors, the capacitance of the sensor varies when human fingers approach or leave. Since the human body could not remain still, the distance between it and the sensor changes slightly, resulting in a subtle proximity response and thus leading to the unstable baseline of the capacitance curve. Because we use the relative capacitance change value as the y-axis, the sensing signals sometimes appear above the zero-tick mark and sometimes below the zero-tick mark. Fig. 4l shows a zoomed-in image of one pulse, from which three characteristic peaks can be observed. Most of the recorded radial pulse waveforms have three distinct peaks, the percussion wave (P-wave, P_1), tidal wave (T-wave, P_2), and diastolic wave (D-wave, P_3). The P-wave and T-wave are related to blood pressure, while the D-wave is related to heart rate.^{44,45} The radial augmentation index ($AI_r = P_2/P_1$), digital volume pulse time ($\Delta T_{DVP} = t_{P2} - t_{P1}$), and diastolic augmentation index ($DAI_r = P_3/P_1$) were calculated as 0.62, 0.23, and 0.22, which are important values for the facile and non-invasive diagnosis of arterial stiffness.^{46,47}

2.4 Crosstalk-free sensing of proximity/pressure

To study the response switching between the proximity and pressure sensing modes, we measured the C_m change in different processes for three cycles. The pressure test platform was used to change the distance between the sensor and the metal rod (simulating a human hand) and record the pressure brought by contact. The whole process included (I) approaching, (II) touching without force, (III) pressing, (IV) releasing pressure and finally (V) leaving the sensor, which is clearly shown in the insets of Fig. 5a. The distances between the finger and sensor together with the pressures applied to the sensor are also listed in the insets. Among these processes, (I) and (V) indicate that a finger is 1 mm away from the sensor surface, (II) and (IV) mean that a finger just touches the surface without pressure, while (III) shows that a finger is pressing down by 1 mm with a pressure of 25.5 kPa. We can detect the turning points (II and IV) to understand the current state of the sensor to switch between proximity and pressure modes, which is of great significance for accurate sensing in practical applications. To clarify how the turning point works, we placed a small leaf with an area of 1.2 cm^2 on the sensor and then took it away after 3 seconds, which induced an intense capacitance change of $\sim 5\%$ (Fig. 5b). The process can be listed as follows: (1) a human hand approaches the sensor with a small leaf; (2) the leaf that is still held in the hand is pressing the sensor; (3) the leaf is lying on the sensor; (4) the leaf is being taken away; (5) the human hand is moving away from the sensor. Notably, T and T' function as the turning points of the proximity and

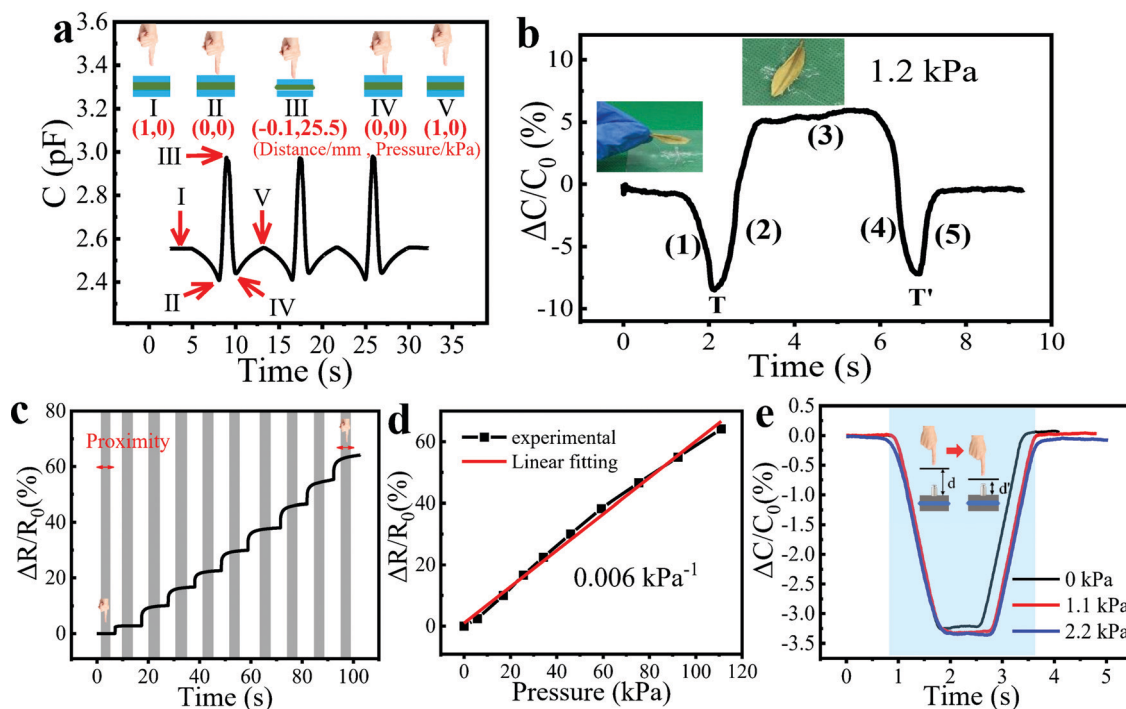


Fig. 5 Crosstalk-free sensing of proximity/pressure. (a) Response switching between the proximity and pressure sensing modes for 3 cycles. Insets: Processes of the finger (I) approaching, (II) touching without force, (III) pressing, (IV) releasing pressure, and finally (V) leaving the sensor; the first and second numbers in the parentheses are the distances between the fingers and sensor and the pressure applied on the sensor, respectively. (b) Relative capacitance changes when a leaf was put on the sensor and then taken away by a hand: (1) response induced by an approaching human hand; (2) a leaf is gradually pressing the sensor; (3) the leaf is lying on the sensor; (4) the leaf is being taken away and (5) response induced by a leaving human hand. Insets: Pictures of the leaf approaching to the sensor by hand and the leaf lying on the sensor. (c) Dynamic resistance response of the pressure sensor to various pressures from 0 to 110 kPa with the proximity of a finger during the test (marked with gray color). (d) Resistance response variation of the sensor vs. pressure. (e) Dynamic capacitance response of the proximity sensor to an approaching finger under the pressures of 0, 1.1, and 2.2 kPa, showing that the proximity sensor can work normally under different pressures.

pressure modes, clearly illustrating the moments when the leaf is touching and leaving the sensor.

How proximity and pressure sensing interfere with each other was also explored. We measured the dynamic resistance response of the pressure sensor to pressures from 0 to 110 kPa with the proximity of a finger during the test (Fig. 5c). The resistance of the sensor did not change when the human hand approached the sensor, which can be seen more clearly in Fig. S7 (ESI†). Thanks to the insensitivity of resistance to the proximity of the finger, the resistance mode can be used for crosstalk-free measurement of pressure, and the correction of the proximity and pressure measured in capacitance mode. In Fig. 5d, the relative resistance variation showed good linearity to the pressure change. Note that the pressure sensitivity in resistance mode was calculated as 0.006 kPa^{-1} , which was much less than that in the capacitance mode (0.91 kPa^{-1}). In addition, we placed different weights on the sensor and conducted proximity tests. The results showed that the different weights on the sensor did not affect the normal operation of the proximity sensor (Fig. 5e).

2.5 Proximity/pressure sensing under strains and after damage

When the sensor is applied to flexible robots or wearable devices, it is likely to be stretched during the movement of

the equipment or human body. Therefore, whether the sensor possesses enough elasticity to adapt to the strain of the robot and work normally under tensile conditions needs further investigation. Fortunately, attributed to the excellent deformability of the hydrogel fibers and Ecoflex film, the bimodal sensors are capable of working under 100% strain without degrading the sensing performance. Here, we utilized a homemade tensile machine to stretch the bimodal sensor during the proximity/pressure sensing and a metal rod to simulate the approach of a human hand with the aid of a displacement platform to control the movement of the metal rod (Fig. S8, ESI†). In the initial state, the metal rod merely touched the sensor without pressure, and then gradually moved away. As shown in Fig. 6a, the curves of proximity sensing almost coincided with the presence of stretching within the strain range of 0 to 90%, indicating the excellent insensitivity to strain. Also, when the distance between the metal rod and the sensor was fixed, the capacitance response remained almost constant as the strain increased (Fig. 6b). This is probably because the proximity response depends primarily on the initial capacitance of the sensor, the capacitance of the approaching object, and the distance between the sensor and object. As shown in Fig. S9 (ESI†), strains had a small effect on the initial capacitance of the sensor. The capacitance change of the sensor was less than 3.7% at 100% tensile strain. This was because when the sensor was

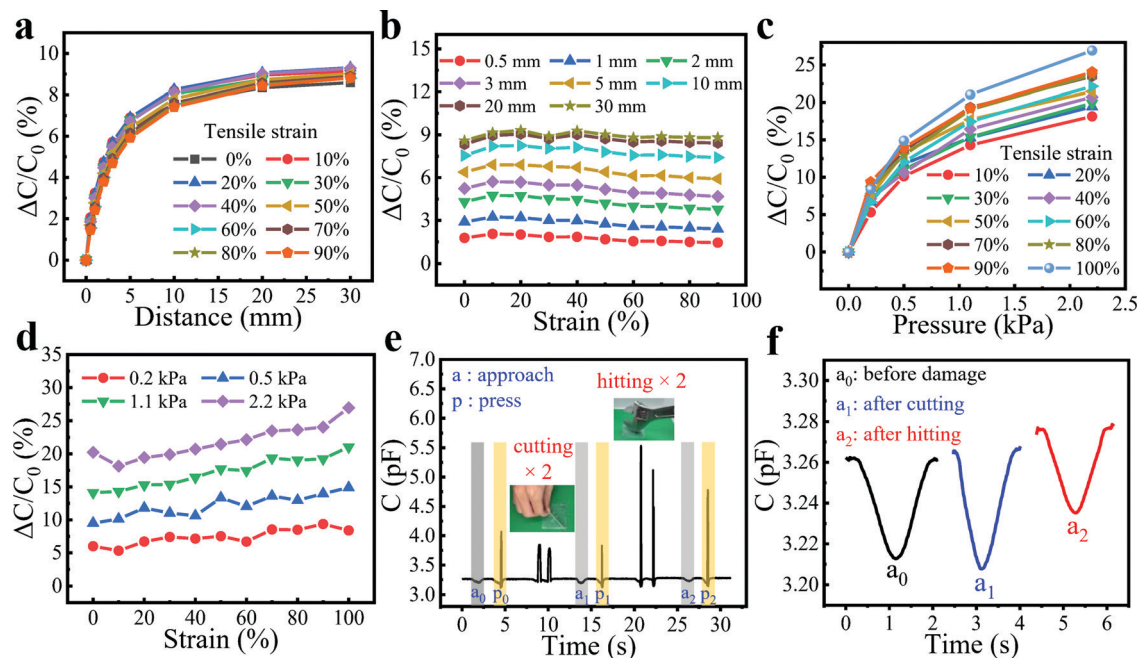


Fig. 6 The proximity/pressure sensing under tensile strain and after damage. (a) Relative capacitance changes responding to an approaching finger under different strains. (b) Relative capacitance change versus strain at different distances between the finger and sensor. (c) Relative capacitance changes responding to pressures under different strains. (d) Relative capacitance changes versus strain under different pressures. (e) Real-time capacitance changes in response to the approach and pressing of a finger before and after damage with a knife and wrench. Insets: Photos showing the knife-cutting and the wrench-hitting. (f) Magnified images of the capacitance changes responding to the approaching hand before and after damage.

stretched, the distance d and the overlap area S of the capacitor decreased at the same time, and by a similar degree, leading to the small change of the initial capacitance. Also, the capacitance of the approaching object and the distance between the sensor and object remained constant, leading to the nearly unchanged proximity response at different strains.

The pressure responses of the sensor under different tensile states were also examined. In Fig. 6c and d, the pressure sensing of the bimodal sensor not only worked normally under a larger strain but also showed a positive effect on its pressure response with the increase of strain. For example, as the strain increased from 0 to 100%, the response to 2.2 kPa was elevated from 18% to 27%. This may be attributed to the fact that the thickness of the Ecoflex between fibers (d) and the overlap area (S) becomes smaller after stretching. When pressure is applied, the degree of further reduction is limited because d is relatively small, while the previously reduced S can be increased to a greater degree, resulting in a greater pressure response. In addition, our bimodal sensor exhibited a remarkable ability to tolerate different kinds of situations intended to test the damage resistance and robustness, including punctures with a knife and smashes from a wrench (Fig. 6e and Movie S6, ESI†). As can be seen from the area of a_0 and p_0 , the bimodal sensor worked normally upon the application of proximity and the pressure of a finger. Then, the sensor was stabbed by a knife twice, which showed no influence on the proximity and pressure sensing capability of the sensor (a_1 and p_1). Finally, the sensor was hit twice with a wrench. Amazingly, the sensor remained functional (a_2 and p_2) after these damages,

demonstrating excellent resilience and robustness. Among them, since the pressure response of the sensor is much larger than the proximity response, the proximity responses of the three cases (a_0 , a_1 , and a_2) are extracted separately. Fig. 6f shows that the proximity response was similar before and after damage, showing good stability of the sensor. The advantages of the sensor's ability to work under large strains and maintain stable operation after various injuries render it promising for application under harsh environments.

3. Conclusions

In conclusion, we have successfully prepared a stretchable, crosstalk-free, resilient, and transparent hydrogel fiber-based bimodal sensor, which was synthesized through a template coupled with a facile dipping strategy. The bimodal sensor displays excellent proximity sensing ability, including high sensitivity ($3.17\% \text{ cm}^{-1}$), wide working range (18 cm), fast response/recovery speed (90/90 ms), and good stability. These impressive performances endow it with the ability to distinguish the finger number and different gestures. Also, as a pressure sensor, it provides high sensitivity (0.91 kPa^{-1}), fast response/recovery speed (40/40 ms), low detection limit (63 Pa), and good linearity due to the elasticity of both the hydrogel and the dielectric layer. Therefore, the wearable sensor can monitor various physiological features with details and high accuracies, such as wrist pulse, vocalization, and swallowing by directly attaching to human skin, demonstrating the great potential to

detect some physiological conditions such as dysphagia and cardiovascular diseases in a non-invasive way. Meanwhile, the sensor units can be utilized for a sensor array, which can realize accurate spatial sensing, pressure mapping, and location identification. Moreover, in addition to understanding the current mode by detecting the turning point of the capacitive response curve toward proximity and pressure, our sensor successfully realized crosstalk-free and multifunctional sensing of proximity/pressure. Attributed to the excellent deformability of the hydrogel fiber, the bimodal sensors were capable of working under 100% strain without degrading the sensing performance. The proximity sensor presented good insensitivity to the applied strain, while the pressure sensitivity was even promoted. Furthermore, with the high resilience of Ecoflex, the bimodal sensor was endowed with good tolerance to outer damage, enabling it to work normally after damage by a knife and a wrench. This ultrasensitive, tough, bimodal sensor fully presents attractive advantages in accurate proximity/pressure detection even in a highly stretched state, and can be an ideal candidate in the fields of wearable electronics, the internet of things, soft robots, and HMI systems.

4. Experimental section

Synthesis of the hydrogel fibers

2.42 g of AAm, 1.45 mg of MBA, 14.5 mg of AP, and 0.3 g of sodium alginate were added to 14 mL of deionized water and stirred for one hour to obtain the precursor solution. The precursor solution was injected into a glass capillary with a diameter of 0.9 mm, and the two ends of the capillary were sealed and heated at 65 °C for two hours to obtain hydrogel fibers. Then, the fibers were taken out from the glass capillary and soaked in 1 M CaCl₂ for 30 min. Finally, the fibers were soaked in 50 wt% LiBr for 15 min to improve the anti-drying ability of the hydrogel fibers.

Fabrication and characterization of the bimodal hydrogel fiber sensor

Firstly, Ecoflex prepolymer was obtained by mixing Ecoflex A and B components at a ratio of 1:1. Then, the Ecoflex prepolymer was spin-coated on several 5 × 5 cm glass sheets at the speed of 400 rpm for 40 s to obtain the elastomer film after its natural condensation. The hydrogel fibers with silver wires tied at both ends were dipped into the Ecoflex prepolymer and taken out after 30 min to form the encapsulation layer of Ecoflex. Then, the two aforementioned fibers were placed perpendicular to each other on the Ecoflex film and fixed to the film with Ecoflex prepolymer to avoid the slippage of the two fibers when the film was stretched. The bimodal fiber sensor can be obtained through the above steps.

Fabrication of the 3 × 3 capacitive sensor array

First, the Ecoflex prepolymer was spin-coated on a 10 cm × 10 cm glass sheet at a speed of 400 rpm for 40 s to obtain two Ecoflex films that would be used in the package of the sensor.

Then, each side of the six hydrogel fibers was tied with silver wires, which were embedded in copper foil to facilitate subsequent measurements. Three hydrogel fibers were placed parallelly on the Ecoflex film and coated with an Ecoflex prepolymer as an insulating layer for the hydrogel fibers. After the curing of the Ecoflex prepolymer, three other identical hydrogel fibers were placed on the insulating layer orthogonally to the original fibers and coated with Ecoflex prepolymer again. Finally, the Ecoflex film was placed on top of it to get the 3 × 3 sensor array.

Device characterization

The capacitance was recorded using an LCR meter (Tonghui Electronic Co. Ltd 2832) with a maximum voltage of 1 V and a 200 kHz sinusoidal signal. The pressure sensing tests were performed on a homemade motorized moving stage (Zolix, SC300-1B) and the force applied to the sensor was recorded using a force gauge (HANDPI Co. Ltd, HP). The strain sensing tests were performed on a tensile machine.

Conflicts of interest

The authors declare no conflicts of interest.

Acknowledgements

J. W. acknowledges financial support from the National Natural Science Foundation of China (61801525), the Guangdong Basic and Applied Basic Research Foundation (2020A1515010693), Fundamental Research Funds for the Central Universities, Sun Yat-sen University (22lgqb17), and the Science and Technology Program of Guangzhou (201904010456).

References

- 1 D. Rus and M. T. Tolley, *Nature*, 2015, **521**, 467–475.
- 2 S. Li, H. Zhao and R. F. Shepherd, *MRS Bull.*, 2017, **42**, 138–142.
- 3 L. Chen, Z. Wang, Z. Zhan, M. Xie, G. Duan, P. Cheng, Y. Chen and H. Duan, *Mater. Today Phys.*, 2021, **19**, 100404.
- 4 X. Wu, Y. Han, X. Zhang, Z. Zhou and C. Lu, *Adv. Funct. Mater.*, 2016, **26**, 6246–6256.
- 5 J. Cao, C. Lu, J. Zhuang, M. Liu, X. Zhang, Y. Yu and Q. Tao, *Angew. Chem.*, 2017, **129**, 8921–8926.
- 6 H. Chang, S. Kim, S. Jin, S.-W. Lee, G.-T. Yang, K.-Y. Lee and H. Yi, *ACS Appl. Mater. Interfaces*, 2018, **10**, 1067–1076.
- 7 S. Jung, J. H. Kim, J. Kim, S. Choi, J. Lee, I. Park, T. Hyeon and D.-H. Kim, *Adv. Mater.*, 2014, **26**, 4825–4830.
- 8 Z. Wang, S. Guo, H. Li, B. Wang, Y. Sun, Z. Xu, X. Chen, K. Wu, X. Zhang, F. Xing, L. Li and W. Hu, *Adv. Mater.*, 2019, **31**, 1805630.
- 9 L. Shi, Z. Li, M. Chen, Y. Qin, Y. Jiang and L. Wu, *Nat. Commun.*, 2020, **11**, 3529.
- 10 Z. Wang, S. Wang, J. Zeng, X. Ren, A. J. Chee, B. Y. Yiu, W. C. Chung, Y. Yang, A. C. Yu, R. C. Roberts, A. C. Tsang, K. W. Chow and P. K. Chan, *Small*, 2016, **12**, 3827–3836.

- 11 B. Zhang, Z. Xiang, S. Zhu, Q. Hu, Y. Cao, J. Zhong, Q. Zhong, B. Wang, Y. Fang, B. Hu, J. Zhou and Z. Wang, *Nano Res.*, 2014, **7**, 1488–1496.
- 12 N. Zhang and Y. Li, *Int. J. Environ. Res. Public Health*, 2018, **15**, 1699.
- 13 S. L. Warnes, Z. R. Little and C. W. Keevil, *mBio*, 2015, **6**, e01697–e01615.
- 14 Y. Ye, C. Zhang, C. He, X. Wang, J. Huang and J. Deng, *IEEE Access*, 2020, **8**, 45325–45342.
- 15 V. Kedambaimoole, N. Kumar, V. Shirhatti, S. Nuthalapati, S. Kumar, M. M. Nayak, P. Sen, D. Akinwande and K. Rajanna, *Adv. Electron. Mater.*, 2021, **7**, 2001214.
- 16 L. Ding, Y. Wang, C. Sun, Q. Shu, T. Hu, S. Xuan and X. Gong, *ACS Appl. Mater. Interfaces*, 2020, **12**, 20955–20964.
- 17 E.-C. Chen, S.-R. Tseng, J.-H. Ju, C.-M. Yang, H.-F. Meng, S.-F. Horng and C.-F. Shu, *Appl. Phys. Lett.*, 2008, **93**, 294.
- 18 H. Guo, Y. J. Tan, G. Chen, Z. Wang, G. J. Susanto, H. H. See, Z. Yang, Z. W. Lim, L. Yang and B. C. K. Tee, *Nat. Commun.*, 2020, **11**, 5747.
- 19 M. R. Kulkarni, R. A. John, M. Rajput, N. Tiwari, N. Yantara, A. C. Nguyen and N. Mathews, *ACS Appl. Mater. Interfaces*, 2017, **9**, 15015–15021.
- 20 F. Guan, Y. Xie, H. Wu, Y. Meng, Y. Shi, M. Gao, Z. Zhang, S. Chen, Y. Chen, H. Wang and Q. Pei, *ACS Nano*, 2020, **14**, 15428–15439.
- 21 P. Zhao, R. Zhang, Y. Tong, X. Zhao, T. Zhang, Q. Tang and Y. Liu, *ACS Appl. Mater. Interfaces*, 2020, **12**, 55083–55093.
- 22 J. Wang, M.-F. Lin, S. Park and P. S. Lee, *Mater. Today*, 2018, **21**, 508–526.
- 23 B. Lee, J. Y. Oh, H. Cho, C. W. Joo, H. Yoon, S. Jeong, E. Oh, J. Byun, H. Kim, S. Lee, J. Seo, C. W. Park, S. Choi, N. M. Park, S. Y. Kang, C. S. Hwang, S. D. Ahn, J. I. Lee and Y. Hong, *Nat. Commun.*, 2020, **11**, 663.
- 24 T. Q. Trung and N.-E. Lee, *J. Mater. Chem. C*, 2017, **5**, 2202–2222.
- 25 M. S. Sarwar, Y. Dobashi, C. Preston, J. K. Wyss, S. Mirabbasi and J. D. W. Madden, *Sci. Adv.*, 2017, **3**, e1602200.
- 26 Y. Cai, J. Shen, C.-W. Yang, Y. Wan, H.-L. Tang, A. A. Aljarb, C. Chen, J.-H. Fu, X. Wei, K.-W. Huang, Y. Han, S. J. Jonas, X. Dong and V. Tung, *Sci. Adv.*, 2020, **6**, eabb5367.
- 27 J. O. Kim, S. Y. Kwon, Y. Kim, H. B. Choi, J. C. Yang, J. Oh, H. S. Lee, J. Y. Sim, S. Ryu and S. Park, *ACS Appl. Mater. Interfaces*, 2019, **11**, 1503–1511.
- 28 Y. Liang, Z. Wu, Y. Wei, Q. Ding, M. Zilberman, K. Tao, X. Xie and J. Wu, *Nano-Micro Lett.*, 2022, **14**, 1–19.
- 29 K. Tao, Z. Chen, J. Yu, H. Zeng, J. Wu, Z. Wu, Q. Jia, P. Li, Y. Fu and H. Chang, *Adv. Sci.*, 2022, 2104168.
- 30 Z. Wu, Q. Ding, Z. Li, Z. Zhou, L. Luo, K. Tao, X. Xie and J. Wu, *Sci. China Mater.*, 2022, **65**(1), DOI: [10.1007/s40843-021-2022-1](https://doi.org/10.1007/s40843-021-2022-1).
- 31 Y. Wei, H. Wang, Q. Ding, Z. Wu, H. Zhang, K. Tao, X. Xie and J. Wu, *Mater. Horiz.*, 2022, DOI: [10.1039/D2MH00284A](https://doi.org/10.1039/D2MH00284A).
- 32 Z. Wu, H. Ding, K. Tao, Y. Wei, X. Gui, W. Shi, X. Xie and J. Wu, *ACS Appl. Mater. Interfaces*, 2021, **13**, 21854–21864.
- 33 Z. Wu, X. Yang and J. Wu, *ACS Appl. Mater. Interfaces*, 2021, **13**, 2128–2144.
- 34 Z. Wu, W. Shi, H. Ding, B. Zhong, W. Huang, Y. Zhou, X. Gui, X. Xie and J. Wu, *J. Mater. Chem. C*, 2021, **9**, 13668–13679.
- 35 Q. Ding, Z. Wu, K. Tao, Y. Wei, W. Wang, B.-R. Yang, X. Xie and J. Wu, *Mater. Horiz.*, 2022, DOI: [10.1039/d1mh01871j](https://doi.org/10.1039/d1mh01871j).
- 36 Y. Jian, S. Handschuh-Wang, J. Zhang, W. Lu, X. Zhou and T. Chen, *Mater. Horiz.*, 2021, **8**, 351–369.
- 37 H. Wang, Y. Zhang, X. Liang and Y. Zhang, *ACS Nano*, 2021, **15**, 12497–12508.
- 38 J. Y. Sun, X. Zhao, W. R. Illeperuma, O. Chaudhuri, K. H. Oh, D. J. Mooney, J. J. Vlassak and Z. Suo, *Nature*, 2012, **489**, 133–136.
- 39 Z. Lei and P. Wu, *Mater. Horiz.*, 2019, **6**, 538–545.
- 40 R. S. Johansson and J. R. Flanagan, *Nat. Rev. Neurosci.*, 2009, **10**, 345–359.
- 41 D. L. Cohen, C. Roffe, J. Beavan, B. Blackett, C. A. Fairfield, S. Hamdy, D. Havard, M. McFarlane, C. McLaughlin, M. Randall, K. Robson, P. Scutt, C. Smith, D. Smithard, N. Sprigg, A. Warusevitane, C. Watkins, L. Woodhouse and P. M. Bath, *Int. J. Stroke*, 2016, **11**, 399–411.
- 42 L. Sura, A. Madhavan, G. Carnaby and M. A. Crary, *Clin. Interventions Aging*, 2012, **7**, 287.
- 43 N. Luo, W. Dai, C. Li, Z. Zhou, L. Lu, C. C. Poon, S. C. Chen, Y. Zhang and N. Zhao, *Adv. Funct. Mater.*, 2016, **26**, 1178–1187.
- 44 Z. Wang, L. Zhang, J. Liu, H. Jiang and C. Li, *Nanoscale*, 2018, **10**, 10691–10698.
- 45 Y. Qiao, Y. Wang, H. Tian, M. Li, J. Jian, Y. Wei, Y. Tian, D.-Y. Wang, Y. Pang and X. Geng, *ACS Nano*, 2018, **12**, 8839–8846.
- 46 W. W. Nichols, *Am. J. Hypertens.*, 2005, **18**, 3S–10S.
- 47 Y. Lee, J. Park, S. Cho, Y.-E. Shin, H. Lee, J. Kim, J. Myoung, S. Cho, S. Kang and C. Baig, *ACS Nano*, 2018, **12**, 4045–4054.